Advanced Powder Technology xxx (2018) xxx–xxx

Contents lists available at ScienceDirect

Advanced Powder Technology

journal homepage: www.elsevier.com/locate/apt

Original Research Paper

A new image processing algorithm for three-dimensional angular velocity measurement and its application in a granular avalanche

Cheng-Chuan Lin, Fu-Ling Yang *

Department of Mechanical Engineering, National Taiwan University, Taipei, Taiwan

ARTICLE INFO

Article history:
Received 28 December 2017
Received in revised form 28 January 2018
Accepted 5 February 2018
Available online xxxx

Keywords:
Grain rotation
Dense granular flow
Image processing technique
Granular avalanche

ABSTRACT

This work proposes a novel algorithm to extract three-dimensional angular velocity of a sphere from a sequence of high-speed digital images of this sphere and its marker stickers. This technique can capture the angular velocity $\boldsymbol{\omega}$ of a sphere made to move at a specific angle from the camera by an offset DC motor and its speed $|\boldsymbol{\omega}|$ with an error lower than 5%. The method is then applied to measure individual grain rotation dynamics at the boundary during a bulk avalanche to extract the instantaneous contour of each angular velocity component which is in qualitative agreement to that reported from a complementing discrete element simulation. The angular velocity of individual grains $|\boldsymbol{\omega}_p|$ is further analyzed with its local packing density and configuration to confirm that the sudden rise of $|\boldsymbol{\omega}_p|$ is always accompanied by local dilatation upon particle rearrangement.

1. Introduction

Granular flows have been extensively investigated in recent years for its common occurrence in natural hazards and industrial processes with a focus on developing a constitutive relation to describe the rich multi-phasic behaviors under different flow conditions. Since these models treat the bulk as a continuum, the constitutive relations are often expressed in terms of macroscopic flow properties without explicit relation with the detail of grain interaction. The only exception is the model developed from the kinetic theory in the collisional regime in which the information carried at the grain size scale is all embedded in the transport coefficients and their dependence on granular temperature. However, how to extend this approach for flow in the dense and quasi-static regime remains an ongoing research topic. While the granular temperature measures the strength of heterogeneity in local individual grain motion, the likeness of grain motion was exploited to estimate a correlation length scale to indicate how far a disturbance can propagate through interaction force network. Nonetheless, it remains an ongoing research topic to clarify how the constitutive relation in the dense and quasi-static flow regimes depend on these two variables and another inertial number, I, has been discovered to describe bulk friction coefficient by the recently renown $\mu(I)$ relation.

The success of the kinetic theory model in the collisional regime and the $\mu(I)$ model in the dense and quasi-static regime may both be attributed to a successful correlation to the essential micromechanics in each flow regime. It hence is intriguing to ask if there is other micro-mechanism shall be considered in modeling the bulk macro-mechanical behavior and grain rotation, in fact, has been considered in various aspects [1–6]. In the quasi-static regime, Calvetti et al. [7] measured the rotation of two-dimensional (2D) wooden rollers in simple shear and found the standard deviation of the rotation distribution increases with strain. Grain rotation is also shown to play a crucial role in the formation of shear bands [8–12]. Furthermore, when Da Cruz et al. [13] report the monotonically increasing $\mu(I)$ relation from a 2D discrete element simulation of simple shear flows, they also detected that most disks were in rolling contact. Grain rotation was also observed at the lateral boundary when granular avalanche of finite mass was generated on an inclined flume [14]. This micro-mechanism was employed by Yang and Huang [15] to explain why the bulk effective wall friction coefficient μ_w decays in depth from a three-dimensional (3D) discrete element simulation which decay is also reported from 3D steady flow simulation (Richard et al. [16], Bordu et al. [17] and Artoni et al. [18]). Though grain rotation provides rich information to advance our understanding of granular flow dynamics, a reliable measurement technique is yet unavailable. Hence, the objective of this work is to propose a novel image-based algorithm to measure three-dimensional angular velocity of a sphere when it moves at the flow boundary. Section 2 describes the algorithm which is

* Corresponding author.
E-mail address: fulingyang@ntu.edu.tw (F.-L. Yang).

https://doi.org/10.1016/j.apt.2018.02.004
0921-8831/

evaluated and validated in Section 3. We then applied the technique to study the rotation dynamics of a wall layer of a bulk in avalanche to provide experimental evidence to the simulation results of Yang and Huang [19]. Section 5 summarizes the features of this rotation measurement algorithm and discuss possible future applications and enhancement.

2. Algorithm

2.1. Image processing for sphere and sticker locations

Fig. 1(a) shows the study object for algorithm calibration and application experiments on which several circular stickers were glued over the sphere surface as the markers for angular speed measurement. Sufficiently many markers are required to make sure that at least one sticker can be captured in each image during the observation and the specific information will be provided in later context. We will first introduce the algorithm for angular speed measurement and then describe how the required variables are extracted. To measure the angular velocity, the locations of both the sphere and the marker in each image should be known a priori which is obtained by the method of Circular Hough Transformation [20] as introduced in the following.

Let $A(x_1, y_1)$ be a point on the circumference of a circle $(x-a)^2+(y-b)^2=r^2$ whose center (a,b) and radius r are desired as illustrated in Fig. 1(b). By rewriting the circle formula into $(a-x_1)^2+(b-y_1)^2-r^2=0$, we may interpret (x_1,y_1) as the tip of an inversed circular cone in the $a-b-r$ parameter space with $r=0$. In other words, the family of circles of a specific radius r^* that passes A in the physical space would be the circle formed when the horizontal plane $r=r^*$ intersects with the cone as shown in Fig. 1(c). Among the infinitely many circles that pass $A(x_1,y_1)$, the desired circle would correspond to one specific point on the cone (a_0,b_0,r_0) that we pinpoint by the intersection of two other cones standing at $(x_2,y_2,0)$ and $(x_3,y_3,0)$ from the transformation of another two points $B(x_2,y_2)$ and $C(x_3,y_3)$ on the circumference. Upon implementation, we mapped all the circumference points into the parameter space to find (a_0,b_0,r_0) by the point passed the most frequently by all the cones. If there were two parameter points of equal cone-passing counts, we took the average.

The sticker center (x_s,y_s) was located by the same method if we have its full shape. However, Circular Hough Transformation would become imprecise when the sticker moves to the border of sphere in the image and become irregularly non-circular in the image, as those boxed red stickers in Fig. 1(a). Therefore, we turned to use the averaged coordinate of all the N sticker pixels to present the sticker location as $(x_s,y_s)=(\sum x_{pi}/N, \sum y_{pi}/N)$ and these sticker pixels were identified by an index condition. For example, we used green stickers on the white Styrofoam sphere in the calibration experiments and red or green stickers on the blue glass spheres in the avalanche experiments (in Fig. 1(a)) as the RGB indices, $[R_{ind}, G_{ind}, B_{ind}]$, are significantly different for the stickers and the sphere in the color images. To locate all pixels of red stickers on a sphere at (a_0,b_0) with radius r_0, we scanned through a rectangle of vertices $(a_0\pm r_0, b_0)$ and $(a_0, b_0\pm r_0)$ in the image to identify all the local pixels that satisfy the index condition $R_{ind}>G_{ind}+C$ and $R_{ind}>B_{ind}+C$. Here, C must be a sufficiently large threshold value to avoid capturing a grayish pixel with $R_{ind}\approx G_{ind}\approx B_{ind}$ (a nearly white or black pixel possesses $[R_{ind},G_{ind},B_{ind}]=[253,250,251]$ or [27, 20, 23] in our images). An appropriate value of C is crucial and can always be obtained easily with a few trial runs.

2.2. Post analysis for angular velocity

By applying the location algorithms to k ($k=1$–5) consecutive images, we obtain a time sequence of two-dimensional sphere positions (X_k,Y_k) in the laboratory coordinate system and the corresponding three-dimensional sticker positions $S_k(x'_{sk},y'_{sk},z'_{sk})$ in the sphere-fitted coordinate system $x'-y'-z'$. Here, $x'_{sk}=x_{sk}-X_k$, $y'_{sk}=y_{sk}-Y_k$ and $z'_{sk}=[R^2-x'^2_{sk}-y'^2_{sk}]^{1/2}$ with R being the sphere radius (see Fig. 2(a)). If we assume a nearly unchanged rotation axis ψ over the observation period, these consecutive sticker positions shall sweep a short arc in a plane $E: z'=Ax'+By'+C$ perpendicular to ψ as sketched in Fig. 2(b). The novelty of our algorithm is how we extract the surface normal vector $\boldsymbol{n}=(A,B,-1)$ from the consecutive sticker positions S_k and then determine the rotation axis ψ by further requiring the normal vector to pass the sphere center $O(x',y',z')=(0,0,0)$.

To fit $\boldsymbol{n}$ in a least-square sense, we first substitute the sticker positions $S_k(x'_{sk},y'_{sk},z'_{sk})$ for $k=1-n$ into the plane equation E to estimate a total squared residual S_{res} as

$$S_{res}=\sum_{k=1}^{n} r_{res,k}^2, \quad \text{with} \quad r_{res,k}=z'_{sk}-Ax'_{sk}-By'_{sk}-C \tag{1a, b}$$

The best-fitted plane constants (A,B,C) are then determined by those minimize S_{res} and hence the derivatives of S_{res} with respect to each of A, B and C should vanish to give

$$\begin{cases} \frac{\partial S_{res}}{\partial A}=\sum_{k=1}^{n}2(z'_{sk}-Ax'_{sk}-By'_{sk}-C)(-x'_{sk})=0, \\ \frac{\partial S_{res}}{\partial B}=\sum_{k=1}^{n}2(z'_{sk}-Ax'_{sk}-By'_{sk}-C)(-y'_{sk})=0, \\ \frac{\partial S_{res}}{\partial C}=\sum_{k=1}^{n}2(z'_{sk}-Ax'_{sk}-By'_{sk}-C)(-1)=0. \end{cases} \tag{2a, b, c}$$

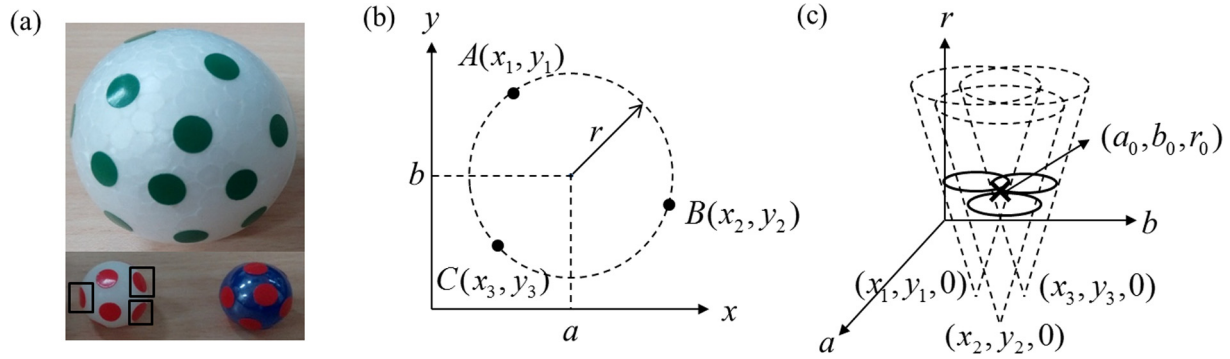

Fig. 1. (a) Experimental spheres stuck with different size (diameter 7 mm and 5 mm) and color (green and red) stickers on its surface. The stickers inside black box demonstrate that the stickers become non-circular shape when they move to the sphere border. (b) Illustration of Circular Hough Transformation for three circumference points $A(x_1,y_1)$, $B(x_2,y_2)$ and $C(x_3,y_3)$ on physical space $x-y$ transformed to (c) threes cones with its vertices $(x_1,y_1,0)$, $(x_2,y_2,0)$ and $(x_3,y_3,0)$ on parameter space $a-b-r$. The intersection point (a_0,b_0,r_0) is the most probable center coordinate and radius of the original circle. (To see the sticker colors in (a), the reader is referred to the web version of this article.)

Please cite this article in press as: C.-C. Lin, F.-L. Yang, A new image processing algorithm for three-dimensional angular velocity measurement and its application in a granular avalanche, Advanced Powder Technology (2018), https://doi.org/10.1016/j.apt.2018.02.004